ADVANCED MATERIALS
www.advmat.de

A Quinonoid-Imine-Enriched Nanostructured Polymer Mediator for Lithium–Sulfur Batteries

*Chen-Yu Chen, Hong-Jie Peng, Ting-Zheng Hou, Pei-Yan Zhai, Bo-Quan Li, Cheng Tang, Wancheng Zhu, Jia-Qi Huang, and Qiang Zhang**

The reversible formation of chemical bonds has potential for tuning multi-electron redox reactions in emerging energy-storage applications, such as lithium–sulfur batteries. The dissolution of polysulfide intermediates, however, results in severe shuttle effect and sluggish electrochemical kinetics. In this study, quinonoid imine is proposed to anchor polysulfides and to facilitate the formation of Li_2S_2/Li_2S through the reversible chemical transition between protonated state (—NH^+=) and deprotonated state (—N=). When serving as the sulfur host, the quinonoid imine-doped graphene affords a very tiny shuttle current of 2.60×10^{-4} mA cm^{-2}, a rapid redox reaction of polysulfide, and therefore improved sulfur utilization and enhanced rate performance. A high areal specific capacity of 3.72 mAh cm^{-2} is achieved at 5.50 mA cm^{-2} on the quinonoid imine-doped graphene based electrode with a high sulfur loading of 3.3 mg cm^{-2}. This strategy sheds a new light on the organic redox mediators for reversible modulation of electrochemical reactions.

Nature provides tremendous inspiration for designing novel chemistry and materials to mimic smart biological systems. For example, the reversible formation of chemical bonds, or corresponding reversible transition between two chemical states, is ubiquitous in nature and inspires various applications.[1] These reversible transitions are, however, not only key to conventional chemistry, such as polymer chemistry, supramolecular chemistry, and reticular chemistry, but are also becoming increasingly important and interesting for the growing areas of energy chemistry based on multi-electron transfer, during which the generation and transformation of intermediate guest molecules are involved, and there is a demand for reversible storage and delivery.

The lithium–sulfur (Li–S) battery represents such an emerging energy storage system, based on the multi-electron transfer between elemental S_8 and Li. The energy density of an Li–S battery is theoretically as high as 2600 Wh kg^{-1}.[2] To enable the full demonstration of such an extreme value, liquid electrolytes are primarily considered, in which highly soluble intermediates, polysulfides (Li_2S_n, n = 4–8), are produced to ease the overall reaction pathways through sequential electron/lithium ion (Li^+)-coupled transferring over the solid–liquid interfaces, and thereby preventing the insurmountable solid–solid conversion between two inherently insulating counterparts of sulfur and lithium sulfides (Li_2S) at room temperature. Nevertheless, side effects are also present on the dissolution of polysulfides, mainly manifesting as the shuttle of polysulfides within the Li–S cell. The shuttle phenomenon not only lowers the efficiency of the battery, but also leads to uncontrolled deposition and irreversible loss of active materials on lithium anode or in other electrical insulating regions. Designing functional separators[3] and anode protection[4] have been successfully demonstrated as efficient and effective strategies to inhibit shuttle phenomenon across the cells. The promotion of interfacial electrochemical kinetics as well as controllable deposition of polysulfides,[5] however, still demands for immobilizing polysulfides on conductive nanostructured cathode hosts, and reversibly delivering polysulfides to proceed electrochemical reactions.

Various nanostructured carbonaceous hosts (e.g., nonpolar graphene, carbon nanotubes, and porous carbon) have been explored to encapsulate sulfur and polysulfides.[6] The physical isolation offered by nonpolar carbon, however, is too weak to bind polar polysulfides. Therefore, the transport of polysulfides, driven by the thermodynamics, leads to the detachment of guest molecules from the host, making the corresponding interfacial redox reaction sluggish.[7] Chemical bonds, either provided by heteroatom-doped carbon,[8,9]

C.-Y. Chen, H.-J. Peng, T.-Z. Hou, P.-Y. Zhai, B.-Q. Li, C. Tang, Prof. J.-Q. Huang, Prof. Q. Zhang
Beijing Key Laboratory of Green Chemical Reaction Engineering and Technology, Department of Chemical Engineering
Tsinghua University
Beijing 100084, P. R. China
E-mail: zhang-qiang@mails.tsinghua.edu.cn
T.-Z. Hou
Department of Materials Science and Engineering
University of California Berkeley
CA 94720, USA
P.-Y. Zhai, Prof. W. Zhu
Department of Chemical Engineering
Qufu Normal University
Shandong 273165, P. R. China
Prof. J.-Q. Huang
Advanced Research Institute for Multidisciplinary Science
Beijing Institute of Technology
Beijing 100081, P. R. China
The ORCID identification number(s) for the author(s) of this article can be found under http://dx.doi.org/10.1002/adma.201606802.

DOI: 10.1002/adma.201606802

conductive polymers (e.g., polypyrrole,[10] polyacrylonitrile,[11] poly(3, 4-ethylenedioxythiophene),[12] and polyaniline[13]), or inorganics (e.g., metal oxides,[5,14,15] hydroxides,[16] sulfides,[17] nitride,[18] and carbide[19,20]), are consequently proposed with diverse mechanisms. As a result of strong anchoring of polysulfides, both high sulfur utilization and long cycling life are usually obtained. Among these polar hosts, several inorganic materials have been regarded efficient polysulfide mediator to regulate the polysulfide redox reactions.[17,19,21,22] Particularly, Nazar and co-workers pioneered the use of MnO_2 to enable a surface-dominant polysulfide redox mechanism through surface-bound polythionate intermediates.[15,22,23] Despite these tremendous efforts, it is still quite challenging for most of the materials to identify the specific role of a certain surface or a functional group among a collection of combinatorial effects offered by different functionalities. The exploration of a unique chemical binding strategy, as well as its combination with controlled nanostructures, is of great interest and importance to probe the complex multi-electron redox reactions between lithium and sulfur. Metal-free polysulfide mediators are especially promising because of the relatively light environmental burden compared to metal compounds. Novel concepts toward the rational design of electrode can therefore be obtained for Li–S batteries.

Very recently, nitrogen atoms, existing in nitrogen-doped nanostructured carbon, play a vital role in anchoring polysulfides.[8,24] For example, the pyridinic- and pyrrolic-N doped in conjugated systems have an extra pair of electrons to naturally act as a Lewis-base site to bind the Lewis acid of terminal lithium atom in Li_2S_x (x = 1–8).[25] Therefore, these two forms of nitrogen atoms are regarded as the most efficient binding sites. However, the organic chemistry reveals the fact that nitrogen-containing functional groups have at least tens of forms. Even a little change in the chemical environment surrounding nitrogen atoms would induce a huge variation in adsorption energetics. Therefore, exploiting undiscovered nitrogen-containing functional groups is in principle possible and would be quite interesting. Precisely tailoring the chemical structure of nitrogen-doped conjugated systems by introducing additional electron saturated or deficient region would create a plenty of opportunities. Constructing desirable nanostructures would further maximize these opportunities.

Here, quinonoid imine (−NH$^+$=/−N=) was for the first time explored as anchoring sites to absorb polysulfides and to enhance Li_2S nucleation with rapid kinetics of polysulfide redox. Enriched quinonoid imine functionalities in the nanostructured polymer were enabled through in situ co-polymerization of aniline and phytic acid (PA) on graphene oxide (GO) (**Figure 1**a). The as-obtained N, P-containing polymer is coated on GO with desirable nanostructures and denoted as NPGO. Samples without PA or GO were also synthesized and denoted as NGO and NP, respectively. The introduction of PA has several advantages, including (1) stabilizing the intermediates during polymerization, (2) promoting the formation of key functional groups of quinonoid imine, (3) allowing crosslinked polymers with robust flexibility and fully exposed anchoring sites, and (4) rendering remarkable enhancement in tuning chemical/physical structures of conductive polymer for being as a polysulfide mediator. During co-polymerization, a portion of amines (−NH−) are oxidized to cations, while simultaneously, the adjacent PA deprotonates to phosphate anions. The electrostatic interaction stabilizes the oxidized amine cation. Subsequently, the π electrons in the conjugated polyaniline rearrange to form a quinonoid structure, while the −NH$^+$= is also stabilized by anionic PA.[26] During electrochemical reactions, quinonoid imine undergoes a reversible transition between the deprotonated state −N= and protonated state −NH$^+$= to bind lithiated/anionic polysulfides, respectively. Such a reversible transformation, triggered by polysulfides, mimics the smart self-healing process found in nature.

The binding of polysulfides (Li_2S_8) on typical N-functionalities, including benzenoid amine (−NH− and −NH_2^+−) and quinonoid imine (−N= and −NH$^+$=) in NPGO, was unveiled through first-principle calculations (Figure 1b). The binding energy of Li_2S_8 to graphene (modeled as coronene) is –1.16 eV. In contrast to the relatively weaker binding to graphene, the Li_2S_8 binds strongly to quinonoid imine (–1.61/–1.83 eV for protonated/deprotonated states). The Li_2S_8 approaches −N= with its positively charged lithium electrostatically trapped by negatively charged nitrogen in quinonoid imine to minimize

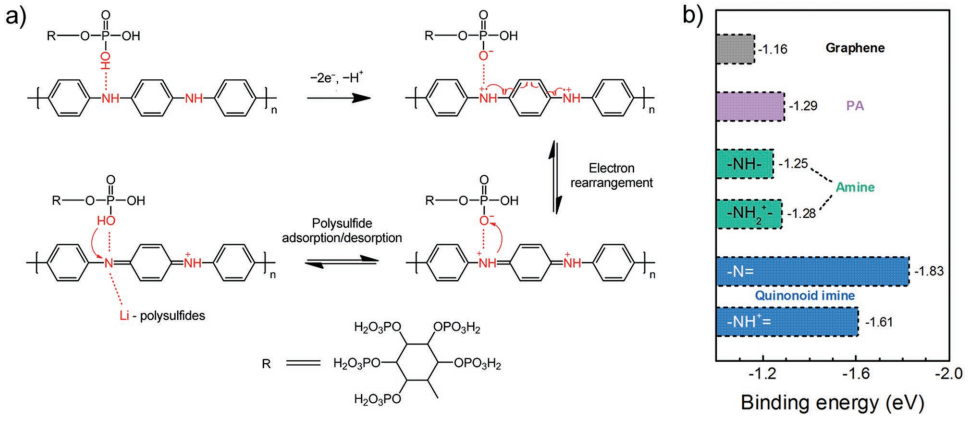

Figure 1. a) Schematic illustrating the stabilization and enrichment of quinonoid imines by PA, as well as the reversible transition between protonated and deprotonated states with simultaneous polysulfide desorption and adsorption. b) Calculated binding energies of a Li_2S_8 molecule on graphene, PA, benzenoid amine (−NH− and −NH_2^+−), and quinonoid imine (−N= and −NH$^+$=) based on density functional theory (DFT).

the overall energy (Figure S1, Supporting Information). Simultaneously, the sulfur chain in Li_2S_8 slightly interacts with the conjugated polymer chain, enabling subsequent charge transfer toward enhanced redox kinetics. For the pronated state, $-NH^+=$, with deprotonated PA counterparts, Li_2S_8 is bound to adjacent negatively-charged phosphate groups. Nevertheless, the difference in their binding energies is only 0.22 eV, which is below the threshold of the 0.25 eV barrier to be energetically favorably overcome at room temperature.[27] Such a thermodynamically surmountable energy penalty validates the reversibility of polysulfide-tuned protonation/deprotonation of quinonoid imine, suggesting the adaptive reusability of anchoring sites. Other N-species such as amine, as well as PA, can only provide limited adsorption to Li_2S_8 with binding energies of –1.25 to –1.29 eV, which is slightly higher than graphene. Therefore, the chemical binding is mainly endowed by quinonoid imine for NPGO to trap polysulfides. Moreover, $-NH^+=$ also provides a binding energy of sulfur (–1.27 eV) comparable to graphene (–1.24 eV), owing to the π–π interaction between sulfur and benzene rings (Figure S2, Supporting Information). The calculation indicates that quinonoid imine favors the adhesion of both polar species (Li_2S_x, $x = 1$–8) and nonpolar species (sulfur).

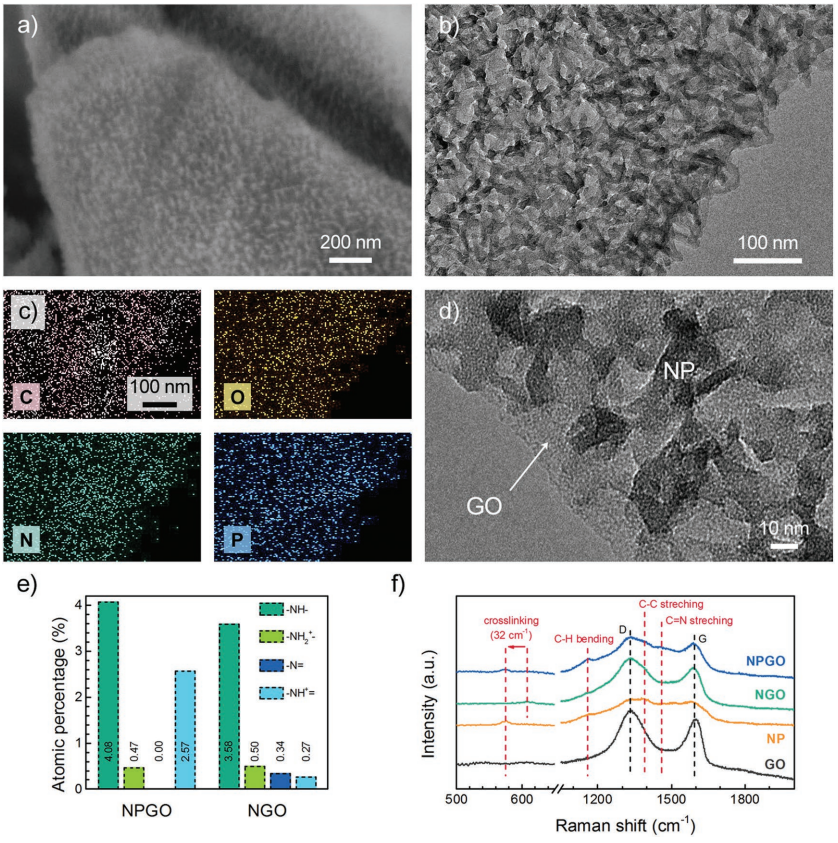

Figure 2. a) Scanning electron microscopy and b,d) transmission electron microscopy images, and c) energy dispersive spectrometric mapping of NPGO; e) distribution of N-species of NPGO and NGO, which is obtained by X-ray photoelectron spectroscopy; f) Raman spectra of NPGO, NGO, NP, and GO.

This promising chemistry was realised by uniformly depositing a nanostructured thin layer of NP on graphene substrate. NPGO was prepared by in situ co-polymerization of aniline and PA on GO in aqueous dispersion at 0 °C for 24.0 h. NGO and NP were also synthesized (Figure S3, Supporting Information). The co-polymer was densely deposited on the surface of GO with a coral-like morphology (**Figure 2**a,b). Dendritic NP was interconnected into a continuous and robust network lying on the GO substrates, which was mainly ascribed to the crosslinking effect of PA (Figure 2b).[28] The uniform distribution of each element also indicates the good dispersion of NP on GO (Figure 2c). Each NP nanorod has a length of ≈50 nm and a diameter of ≈10 nm while the underlying GO is partially exposed (Figure 2d). Such a unique structure allows both rapid transport of electrons from conductive substrates and ions from the electrolyte, as well as the adsorption of reactive intermediates at the boundary between NP and GO. The nanosized feature of NP indicates fully exposed anchoring sites and a great number of the NP/GO/electrolyte interfaces.

The NPGO has an N content of 7.11 at%, much higher than that of NGO (4.70 at%) (Table S1, Supporting Information). As indicated by DFT calculation (Figure S4, Supporting Information), the main reason for such an enhanced nitrogen content is attributed to the electrostatic attraction of oxidized aniline monomers by phosphates in PA. Such an interaction, in principle, also facilitates the protonation of both amine and quinonoid imine as PA donates hydrogen to the Lewis base, namely the conjugated nitrogen. The slightly higher oxygen content of NPGO was resulted from PA. Calculated from the atom percentages of NPGO (Table S1, Supporting Information), the molar ratio of PA and aniline monomer is 1:14.3 in NPGO, and the weight percentage of PA and aniline monomer is 24.3% and 49.0%, respectively.

The various phosphorous and nitrogen components were further determined by fitting the P 2p and N 1s fine scan spectra, respectively (Figure S5, Supporting Information). The P 2p spectra were deconvoluted into two bands at 131.8 eV (P—O) and 133.4 eV (P—C).[29] Only the characteristic of P—O can be found in spectra of NPGO and NP, suggesting the only existence of PA. Four kinds of nitrogen components, namely deprotonated/protonated quinonoid imine (—N=, 397.6 eV; $-NH^+=$, 400.6 eV) and deprotonated/protonated benzenoid amine (—NH—, 399.0 eV; $-NH_2^+-$, 402.1 eV), were confirmed.[30] The —N= was hardly found in NPGO; instead, there was 2.57 at% of its protonated formula, $-NH^+=$, which was significantly higher than the sum of $-NH^+=$ and —N= in NGO (0.61 at%) (Figure 2e). In contrast, the contents of benzenoid amine ($-NH_2^+-$/—NH—) were comparable. Another effect of PA addition was the facilitation of protonation, which agreed well with the DFT calculation (Figure S4, Supporting Information). Therefore, the benefits of PA for enhancing the overall

N-functional groups, quinonoid imine with stronger binding to polysulfides, and the protonated states are shown clearly.

Raman spectra were further employed to identify the chemical structures (Figure 2f). The peaks at ≈1336.5 and ≈1591.5 cm^{-1} are attributed to the D band and G band of graphene, respectively. The peaks at ≈1159.2, ≈1401.8, and ≈1459.8 cm^{-1} are assigned to C—H bending, C—C stretching, and C=N stretching of the quinonoid ring, respectively.[31] These three peaks of NPGO show similar strength to those of NP but are stronger than those of NGO, suggesting that more quinonoid-type rings were formed in NPGO with the presence of PA. The peak at ≈573.7 cm^{-1} is an indication of the crystallization of polyaniline in NGO. However, in NPGO and NP, the corresponding peaks exhibit a red shift of 32 cm^{-1}, which is related to the crosslinking between polyaniline and PA. It indicates that PA, with symmetric distributed phosphate groups, is capable of promoting the formation of a 3D crosslinking structure of polyaniline whereas normal acidic dopants such as H_3PO_4, owing to the topotactic limitation, are unable to stabilize intermolecular structures efficiently.[31] The Fourier transform infrared spectra also confirmed the existence of characteristic N-functionalities and the promotion effect of PA on the formation of quinonoid imine (Figure S6, Supporting Information).

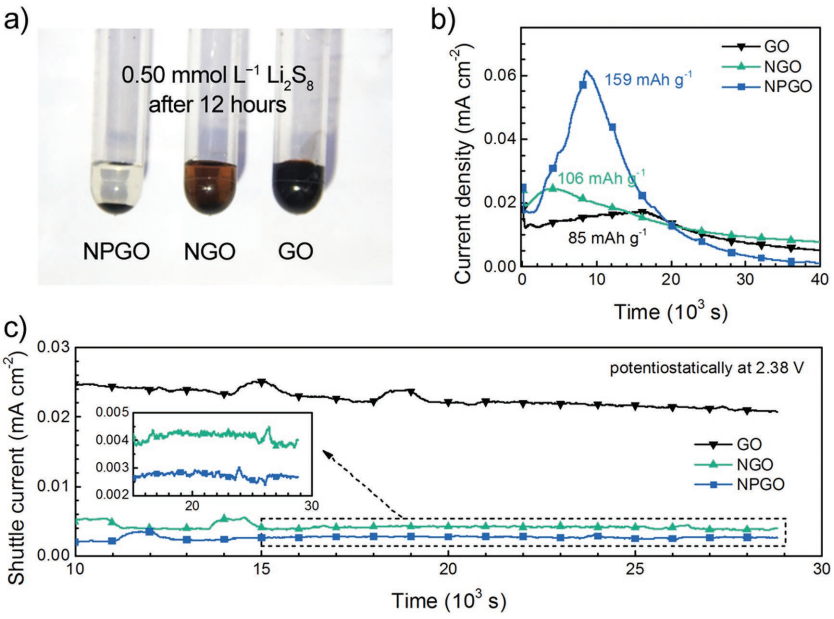

Figure 3. a) Visible adsorption of Li_2S_8 on NPGO, NGO, and GO with the same surface area of 0.8 m^2. b) Potentiostatic discharge curves of Li_2S_8/tetraglyme solution at 2.05 V on different scaffolds with the capacity of Li_2S deposition indicated correspondingly, which is obtained from integral of the current peaks. c) The shuttle currents of Li–S cells with NPGO, NGO, and GO-S cathode.

The strong anchoring of polysulfides by NPGO was confirmed through visible adsorption of 0.5 mmol L^{-1} Li_2S_8 on NPGO, NGO, and GO with the same surface area (0.8 m^2) (**Figure 3**a). The N_2 isotherms of NPGO, NGO, and GO and their specific surface areas determined by Brunauer–Emmett–Teller method are shown in Figure S7, Supporting Information. NPGO possesses a desirable specific surface area of 148 m^2 g^{-1}, which is higher than or comparable to other nanostructured polyanilines.[28] NPGO exhibits the strongest decolorization; while solutions with other additives almost remain the same color as before. Visible adsorption with the same weight of various adsorbents or at higher Li_2S_8 concentration also indicated the strongest adsorptivity of NPGO among these polymer hosts (Figures S8 and S9, Supporting Information).

As we demonstrated before, inorganics (e.g., TiC[19,20]) or inorganic/carbon hybrids (e.g., N-doped graphene/metal hydroxides[21]) with strong adsorption to polysulfides favor the interfacial polysulfide redox and Li_2S deposition. Nevertheless, such an enhancement in reaction kinetics has hardly been unveiled before on polymer mediators. As such, we further monitored the kinetics of Li_2S nucleation by potentiostatically discharging Li_2S_8/tetraglyme catholyte at 2.05 V[19,32] on NPGO, NGO, and GO. Mathematical modeling, following a well-developed method in previous reports,[19,32] was employed to distinguish the contribution of progressive reduction of polysulfides (Li_2S_8 and Li_2S_6) and the precipitation of Li_2S. As shown in Figure 3b, the NPGO exhibits a clear and strong current peak, indicating the efficient deposition of Li_2S. In contrast, similar peaks can rarely be found on NGO and GO. Calculated from the integral of the current density, the capacities of Li_2S precipitation on NPGO, NGO, and GO are 159, 106, and 85 mAh g^{-1}, respectively. More nucleation sites are expected in NPGO, which is attributed to the enriched $-NH^+=$.

The anchoring effect of quinonoid imine also resulted in a reduced shuttle current of the cell with NPGO-S composite cathode (Figure 3c). A potentiostatic charging voltage at 2.38 V was selected as it corresponded to the largest shuttle current in a working Li–S cell.[21,33] The shuttle current of NPGO-S cathode is around 2.60×10^{-4} mA cm^{-2}, which is just a half or one-tenth of that for NGO-S or GO-S cathodes, respectively. It reveals that the NPGO can efficiently adsorb polysulfides and suppress the shuttle effect in a working cell.

The implement of a reversible chemical mediation, provided by enriched quinonoid imine, in Li–S chemistry endowed NPGO-S composite cathode with significantly improved electrochemical behavior. After thermal impregnation, sulfur was uniformly coated on the surface of nanostructured polymer while large sulfur particles were not observed (Figure S10, Supporting Information). As shown in **Figure 4**a, cyclic voltammetric (CV) profiles of both NGO-S and NPGO-S cathodes, which possess comparable sulfur contents (Figure S11, Supporting Information), exhibit typical redox characteristics of Li–S redox. However, the NGO-S possessed much stronger polarization of three CV peaks (≈86 and ≈120 mV for cathodic peaks, corresponding to two-step reduction of sulfur into polysulfides and Li_2S; ≈102 mV for the broad anodic peaks, accounting for reverse reactions) compared to NPGO-S. The inferior electrochemical kinetics of the Li–S asymmetric cell based on NGO-S is in good accordance with the nucleation kinetics results (Figure 3b), which is also attributed to weaker binding on amine than on

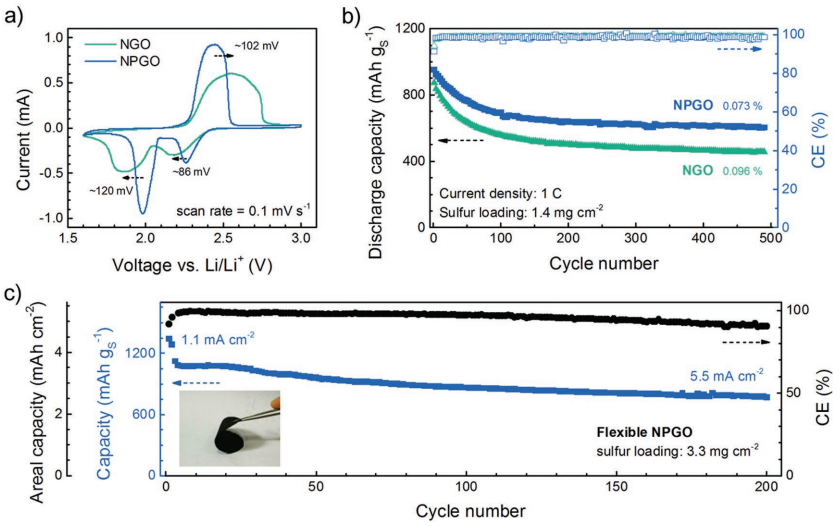

Figure 4. a) CV profiles and b) cycling performance of NPGO and NGO-based S cathodes at 1.0 C; c) cycling performance of a NPGO-S flexible cathode cycled at 5.50 mA cm^{-2} with the inset showing a digital picture of the flexible NPGO-S cathode. CE: Coulombic efficiency.

quinonoid imine, as well as the reduced site density on NGO than on NPGO. These differences in electrochemical kinetics were also reflected in rate capabilities (Figure S12, Supporting Information). At the rate of 2.0 C (1.0 C = 1675 mA g^{-1}), the NPGO-S cathode maintained higher capacity of 570 mAh g^{-1} compared with that of NGO-S (460 mAh g^{-1}) (Figure S12a, Supporting Information). More importantly, the voltage polarization at 2.0 C was also significantly reduced (Figure S12b, Supporting Information). Before and after CV measurements, electrochemical impedance spectra of NPGO-S indicated smaller resistance for charge transferring than those of NGO-S all along (Figure S13, Supporting Information). The reduced polarization, higher utilization at high current densities, and smaller impedance all suggested that by rationally tuning the chemisorption of polysulfides on nanostructured polymer with stronger affinities, the electrochemical kinetics were modulated and reaction rates were promoted.

Due to a more robust crosslinking structure, which stabilizes the interconnected porous scaffolds, and more largely exposed NP/GO/electrolyte interfaces which trap and convert polysulfides, NPGO also enabled enhancement in cycling stability (Figure 4b). At a relatively large current density of 1.0 C, NPGO-S and NGO-S delivered initial capacities of 953 and 873 mAh g^{-1}, respectively, indicating higher utilization of sulfur in NPGO-S. In addition, NPGO-S exhibited reduced cyclic fading rate 0.073% compared to that of NGO-S (0.096%). Note that the initial capacity losses were considerable, which was probably ascribed to poor electrical conductivities of GO substrates. However, reversible capacities were normally attained after 100 cycles, while the capacity of NPGO-S after 500 cycles remained ≈32% higher than that of NGO-S, implying sustainable and reversible electrochemical reactions of sulfur/polysulfides on NPGO. At a low rate of 0.2 C, NPGO-S cathodes also exhibited a high initial discharge capacity of 1114 mAh g^{-1} and retained ≈77% of initial capacity after 100 cycles, which was higher than that of ≈72% at 1.0 C (Figure S14, Supporting Information). The enhanced cycling performance of NPGO-S at low cyclic rate further indicated the importance of electrical conductivity for polar sulfur hosts. After 50 cycles, a dense Li_xS film was coated on the cycled NPGO-S cathode at discharged state as both SEM image and elemental mapping indicated (Figure S15a, Supporting Information). A single sheet of NPGO was also found to be covered by Li_xS deposits (Figure S15b, Supporting Information). Such a postmodern analysis validated the remarkable retention of sulfur species within NPGO-based cathodes.

To enhance the overall electrical conductivity and to attain high energy density of the whole cell, we further fabricated flexible, high areal sulfur loading cathode with NPGO with the assistance of conductive carbon nanotubes (Figure S10c, Supporting Information). With the sulfur loading of 3.3 mg cm^{-2}, it exhibited areal specific capacities of 4.4 and 3.7 mAh cm^{-2} at 0.2 and 1.0 C (1.1 and 5.5 mA cm^{-2}), respectively (Figure 4c). After 200 cycles at large current density of 5.5 mA cm^{-2}, ≈70% of the initial capacity was maintained, indicating that the NPGO with enriched $-NH^+=$ also exerted desirable binding affinities and redox promotion in practical applications of sulfur cathodes. In contrast to sulfur confined in polymer chains with different potentials for sulfur redox reaction in carbonate electrolyte,[11,13,34] the present $-NH^+=$ for anchoring sulfur exhibits high sulfur utilization and excellent stability. The NPGO conductive framework with polar $-NH^+=$ sites is expected to be integrated in sandwich or layer-by-layer structure[35] for cells with higher capacity.

Owing to the relatively low atomic content of $-NH^+=$ (2.57 at%) in NPGO, there might be concerns about whether these anchoring sites are capable of trapping all the soluble polysulfides or not. Theoretically, the molar ratios of elemental sulfur and Li_2S_8 to $-NH^+=/-N=$ sites are 23.3 and 2.91, respectively (Tables S3 and S4, Supporting Information). However, not all of polysulfides have to be immobilized. Actually, the N-functionalities not only help to adsorb the polysulfides, but also facilitate their conversion to Li_2S. Once Li_2S nuclei are formed, polysulfides generated through progressive reduction of sulfur can be adsorbed by and preferentially deposit on these Li_2S nuclei, because Li_2S is also a polar "adsorbent".[20] Therefore, the efficient conversion of polysulfides into polar Li_2S anchors mitigates the aforementioned concern about the amount of anchoring sites.

In conclusion, quinonoid imine is proposed to be a unique anchoring site for polysulfides with the ability of reversible bond formation that mimics natural self-healing systems. A high binding energy can be achieved between Li_2S_8 and quinonoid imine, whereas the two chemical states of quinonoid imine energetically exhibit facile transition, which could be enabled and enhanced by extrinsic Lewis acid/base pair (e.g., PA). NPGO with enriched quinonoid imine was also stabilized through crosslinking from PA. Such a nanostructured polymeric scaffold with deliberately tailored chemical affinities and

fully exposed anchoring sites exhibited strong adsorption to polysulfides, significantly enhanced redox activities, and largely reduced shuttle current. This strategy not only unambiguously probes the specific role of an undiscovered N-containing groups in Li–S batteries, but also sheds a new light on the organic redox mediators for reversible modulation of electrochemical reactions, which can be extended to other cutting-edge applications such as metal-air batteries, redox flow batteries, and electrocatalysis.

Supporting Information

Supporting Information is available from the Wiley Online Library or from the author.

Acknowledgements

C.-Y.C., H.-J.P., and T.-Z.H. contributed equally to this work. This work was supported by funding from National Key Research and Development Program (No. 2016YFA0202500) and Natural Scientific Foundation of China (Nos. 21422604, 21676160, and 21561130151). The authors thank Ze-Wen Zhang, Ge Zhang, Jin Xie, Xiang Chen, and Xin-Bing Cheng for helpful discussions.

Conflict of Interest

The authors declare no conflict of interest.

Keywords

graphene, lithium–sulfur batteries, nanostructure, polysulfides, quinonoid imine

Received: December 16, 2016
Revised: March 1, 2017
Published online:

[1] M. Barboiu, A. M. Stadler, J. M. Lehn, *Angew. Chem., Int. Ed.* **2016**, *55*, 4130.

[2] a) Y.-X. Yin, S. Xin, Y.-G. Guo, L.-J. Wan, *Angew. Chem., Int. Ed.* **2013**, *52*, 13186; b) A. Manthiram, S. H. Chung, C. X. Zu, *Adv. Mater.* **2015**, *27*, 1980; c) H.-J. Peng, X.-B. Cheng, J.-Q. Huang, Q. Zhang, *Adv. Energy Mater.* **2017**, *7*, 1700260; d) Q. Pang, X. Liang, C. Y. Kwok, L. F. Nazar, *Nat. Energy* **2016**, *1*, 16132.

[3] a) J.-Q. Huang, Q. Zhang, F. Wei, *Energy Storage Mater.* **2015**, *1*, 127; b) G. M. Zhou, L. Li, D. W. Wang, X. Y. Shan, S. F. Pei, F. Li, H. M. Cheng, *Adv. Mater.* **2015**, *27*, 641; c) S. H. Chung, A. Manthiram, *Adv. Mater.* **2014**, *26*, 7352.

[4] a) D. Aurbach, E. Pollak, R. Elazari, G. Salitra, C. S. Kelley, J. Affinito, *J. Electrochem. Soc.* **2009**, *156*, A694; b) C. Yan, X.-B. Cheng, C.-Z. Zhao, J.-Q. Huang, S.-T. Yang, Q. Zhang, *J. Power Sources* **2016**, *327*, 212; c) K. Fu, Y. Gong, J. Dai, A. Gong, X. Han, Y. Yao, C. Wang, Y. Wang, Y. Chen, C. Yan, Y. Li, E. D. Wachsman, L. Hu, *Proc. Natl. Acad. Sci. USA* **2016**, *113*, 7094; d) X. B. Cheng, T. Z. Hou, R. Zhang, H. J. Peng, C. Z. Zhao, J. Q. Huang, Q. Zhang, *Adv. Mater.* **2016**, *28*, 2888.

[5] a) X. Y. Tao, J. G. Wang, C. Liu, H. T. Wang, H. B. Yao, G. Y. Zheng, Z. W. Seh, Q. X. Cai, W. Y. Li, G. M. Zhou, C. X. Zu, Y. Cui, *Nat. Commun.* **2016**, *7*, 11203; b) X. Liu, J. Q. Huang, Q. Zhang, L. Q. Mai, *Adv. Mater.* **2017**, *29*, 1601759.

[6] a) J. Liang, Z.-H. Sun, F. Li, H.-M. Cheng, *Energy Storage Mater.* **2016**, *2*, 76; b) Z. W. Seh, Y. Sun, Q. Zhang, Y. Cui, *Chem. Soc. Rev.* **2016**, *45*, 5605; c) Y. H. Xu, Y. Wen, Y. J. Zhu, K. Gaskell, K. A. Cychosz, B. Eichhorn, K. Xu, C. S. Wang, *Adv. Funct. Mater.* **2015**, *25*, 4312; d) M. Li, Y. N. Zhang, X. L. Wang, W. Ahn, J. P. Jiang, K. Feng, G. Lui, Z. W. Chen, *Adv. Funct. Mater.* **2016**, *26*, 8408.

[7] C. J. Hart, M. Cuisinier, X. Liang, D. Kundu, A. Garsuch, L. F. Nazar, *Chem. Commun.* **2015**, *51*, 2308.

[8] a) J. Song, M. L. Gordin, T. Xu, S. Chen, Z. Yu, H. Sohn, J. Lu, Y. Ren, Y. Duan, D. Wang, *Angew. Chem., Int. Ed.* **2015**, *54*, 4325; b) Z. Wang, Y. Dong, H. Li, Z. Zhao, H. Bin Wu, C. Hao, S. Liu, J. Qiu, X. W. Lou, *Nat. Commun.* **2014**, *5*, 5002.

[9] a) C. Tang, Q. Zhang, M. Q. Zhao, J. Q. Huang, X. B. Cheng, G. L. Tian, H. J. Peng, F. Wei, *Adv. Mater.* **2014**, *26*, 6100; b) S. N. Talapaneni, T. H. Hwang, S. H. Je, O. Buyukcakir, J. W. Choi, A. Coskun, *Angew. Chem., Int. Ed.* **2016**, *55*, 3106.

[10] Z. W. Seh, H. Wang, P.-C. Hsu, Q. Zhang, W. Li, G. Zheng, H. Yao, Y. Cui, *Energy Environ. Sci.* **2014**, *7*, 672.

[11] J. L. Wang, J. Yang, J. Y. Xie, N. X. Xu, *Adv. Mater.* **2002**, *14*, 963.

[12] W. Y. Li, G. Y. Zheng, Y. Yang, Z. W. Seh, N. Liu, Y. Cui, *Proc. Natl. Acad. Sci. USA* **2013**, *110*, 7148.

[13] a) J. Yan, B. Li, X. Liu, *Nano Energy* **2015**, *18*, 245; b) G.-C. Li, G.-R. Li, S.-H. Ye, X.-P. Gao, *Adv. Energy Mater.* **2012**, *2*, 1238; c) L. Xiao, Y. Cao, J. Xiao, B. Schwenzer, M. H. Engelhard, L. V. Saraf, Z. Nie, G. J. Exarhos, J. Liu, *Adv. Mater.* **2012**, *24*, 1176.

[14] a) X. Liang, C. Y. Kwok, F. Lodi-Marzano, Q. Pang, M. Cuisinier, H. Huang, C. J. Hart, D. Houtarde, K. Kaup, H. Sommer, T. Brezesinski, J. Janek, L. F. Nazar, *Adv. Energy Mater.* **2016**, *6*, 1501636; b) Q. Fan, W. Liu, Z. Weng, Y. M. Sun, H. L. Wang, *J. Am. Chem. Soc.* **2015**, *137*, 12946.

[15] Z. Li, J. T. Zhang, X. W. Lou, *Angew. Chem., Int. Ed.* **2015**, *54*, 12886.

[16] J. T. Zhang, H. Hu, Z. Li, X. W. Lou, *Angew. Chem., Int. Ed.* **2016**, *55*, 3982.

[17] Z. Yuan, H. J. Peng, T. Z. Hou, J. Q. Huang, C. M. Chen, D. W. Wang, X. B. Cheng, F. Wei, Q. Zhang, *Nano Lett.* **2016**, *16*, 519.

[18] Z. M. Cui, C. X. Zu, W. D. Zhou, A. Manthiram, J. B. Goodenough, *Adv. Mater.* **2016**, *28*, 6926.

[19] H.-J. Peng, G. Zhang, X. Chen, Z.-W. Zhang, W.-T. Xu, J.-Q. Huang, Q. Zhang, *Angew. Chem., Int. Ed.* **2016**, *55*, 12990.

[20] X. Liang, A. Garsuch, L. F. Nazar, *Angew. Chem., Int. Ed.* **2015**, *54*, 3907.

[21] H.-J. Peng, Z.-W. Zhang, J.-Q. Huang, G. Zhang, J. Xie, W.-T. Xu, J.-L. Shi, X. Chen, X.-B. Cheng, Q. Zhang, *Adv. Mater.* **2016**, *28*, 9551.

[22] X. Liang, C. Hart, Q. Pang, A. Garsuch, T. Weiss, L. F. Nazar, *Nat. Commun.* **2015**, *6*, 5682.

[23] X. Wang, G. Li, J. Li, Y. Zhang, A. Wook, A. Yu, Z. Chen, *Energy Environ. Sci.* **2016**, *9*, 2533.

[24] a) Y. Qiu, W. Li, W. Zhao, G. Li, Y. Hou, M. Liu, L. Zhou, F. Ye, H. Li, Z. Wei, S. Yang, W. Duan, Y. Ye, J. Guo, Y. Zhang, *Nano Lett.* **2014**, *14*, 4821; b) H.-J. Peng, T.-Z. Hou, Q. Zhang, J.-Q. Huang, X.-B. Cheng, M.-Q. Guo, Z. Yuan, L.-Y. He, F. Wei, *Adv. Mater. Interfaces* **2014**, *1*, 1400227; c) F. Sun, J. Wang, H. Chen, W. Li, W. Qiao, D. Long, L. Ling, *ACS Appl. Mater. Interfaces* **2013**, *5*, 5630.

[25] T. Z. Hou, X. Chen, H. J. Peng, J. Q. Huang, B. Q. Li, Q. Zhang, B. Li, *Small* **2016**, *12*, 3283.

[26] a) K. Yamamoto, D. Taneichi, *Macromol. Chem. Phys.* **2000**, *201*, 6; b) M. S. Freund, B. A. Deore, *Self-Doped Conducting Polymers*, John Wiley & Sons, Hoboken, NJ, USA **2007**.

[27] J. K. Norskov, F. Studt, F. Abild-Pedersen, T. Bligaard, *Fundamental Concepts in Heterogeneous Catalysis*, John Wiley & Sons, Hoboken, NJ, USA **2014**.

[28] L. Pan, G. Yu, D. Zhai, H. R. Lee, W. Zhao, N. Liu, H. Wang, B. C. K. Tee, Y. Shi, Y. Cui, Z. Bao, *Proc. Natl. Acad. Sci. USA* **2012**, *109*, 9287.
[29] X. Cui, Q. Li, Y. Li, F. Wang, G. Jin, M. Ding, *Appl. Surf. Sci.* **2008**, *255*, 2098.
[30] a) J. Yue, A. J. Epstein, *Macromolecules* **1991**, *24*, 4441; b) J. Joo, J. K. Lee, S. Y. Lee, K. S. Jang, E. J. Oh, A. J. Epstein, *Macromolecules* **2000**, *33*, 5131; c) W. Ding, Z. D. Wei, S. G. Chen, X. Q. Qi, T. Yang, J. S. Hu, D. Wang, L. J. Wan, S. F. Alvi, L. Li, *Angew. Chem., Int. Ed.* **2013**, *52*, 11755.
[31] a) P. Colomban, S. Folch, A. Gruger, *Macromolecules* **1999**, *32*, 3080; b) M. Cochet, G. Louarn, S. Quillard, M. I. Boyer, J. P. Buisson, S. Lefrant, *J. Raman Spectrosc.* **2000**, *31*, 1029.
[32] F. Y. Fan, W. C. Carter, Y. M. Chiang, *Adv. Mater.* **2015**, *27*, 5203.
[33] D. Moy, A. Manivannan, S. R. Narayanan, *J. Electrochem. Soc.* **2015**, *162*, A1.
[34] a) J. L. Wang, Y. S. He, J. Yang, *Adv. Mater.* **2015**, *27*, 569; b) B. C. Duan, W. K. Wang, A. B. Wang, K. G. Yuan, Z. B. Yu, H. L. Zhao, J. Y. Qiu, Y. S. Yang, *J. Mater. Chem. A* **2013**, *1*, 13261; c) W. J. Chung, J. J. Griebel, E. T. Kim, H. Yoon, A. G. Simmonds, H. J. Ji, P. T. Dirlam, R. S. Glass, J. J. Wie, N. A. Nguyen, B. W. Guralnick, J. Park, A. Somogyi, P. Theato, M. E. Mackay, Y. E. Sung, K. Char, J. Pyun, *Nat. Chem.* **2013**, *5*, 518.
[35] a) H. Q. Wang, W. C. Zhang, H. K. Liu, Z. P. Guo, *Angew. Chem., Int. Ed.* **2016**, *55*, 3992; b) L. Qie, A. Manthiram, *Adv. Mater.* **2015**, *27*, 1694; c) R. Fang, S. Zhao, S. Pei, X. Qian, P.-X. Hou, H.-M. Cheng, C. Liu, F. Li, *ACS Nano* **2016**, *10*, 8676.